Improved Hamiltonians for Quantum Simulations of Gauge Theories

Marcela Carena,[1,2,3,4,*] Henry Lamm,[1,†] Ying-Ying Li[1,‡] and Wanqiang Liu[4,§]

[1]*Fermi National Accelerator Laboratory, Batavia, Illinois 60510, USA*
[2]*Enrico Fermi Institute, University of Chicago, Chicago, Illinois 60637, USA*
[3]*Kavli Institute for Cosmological Physics, University of Chicago, Chicago, Illinois 60637, USA*
[4]*Department of Physics, University of Chicago, Chicago, Illinois 60637, USA*

Quantum simulations of lattice gauge theories for the foreseeable future will be hampered by limited resources. The historical success of improved lattice actions in classical simulations strongly suggests that Hamiltonians with improved discretization errors will reduce quantum resources, i.e., require $\gtrsim 2^d$ fewer qubits in quantum simulations for lattices with d-spatial dimensions. In this work, we consider $\mathcal{O}(a^2)$-improved Hamiltonians for pure gauge theories and design the corresponding quantum circuits for its real-time evolution in terms of primitive gates. An explicit demonstration for $\mathbb{Z}_2$ gauge theory is presented including exploratory tests using the ibm_perth device.

Introduction.—Monte Carlo methods in lattice gauge theory (LGT), though powerful in many nonperturbative calculations, can suffer from sign problems—the Boltzmann weight during sampling becomes complex valued—when simulating real-time dynamics. Thus, exponential resources are required to solve many interesting problems in particle physics, such as out-of-equilibrium evolution in the early universe [1], parton distribution function in hadron collisions [2–4], and the shear viscosity of the quark-gluon plasma [5]. Quantum computers can directly perform real-time simulations, avoiding these exponentially large resources plaguing classical methods [6–8]. Quantum simulation in the Hamiltonian formalism evolves the system with the time evolution operator $\hat{U}(t) = e^{-i\hat{H}t}$. A Hamiltonian $\hat{H}$ is constructed at finite lattice spacing a, causing discretization errors compared to the continuum theory in powers of a. Hamiltonians with discretizations scaling with lower powers of a require smaller lattice spacings for the same errors. This implies larger qubit requirements, since the number of qubits is $\mathcal{O}[(L/a)^d]$ for a d-spatial dimensional lattice of length L.

The lattice gauge degrees of freedom, e.g., photons and gluons, need to be rendered finite and mapped to qubits [9–30]. Current estimates for representing SU(3) suggest ~10 qubits per gluon link [11,22,31–35]. Further exacerbating the demand for qubits is the current, noisy status of quantum computers due to, e.g., entanglement with the environment and imperfect evolution. Though it remains an open question how much quantum error correction is required to perform lattice simulations, general estimates suggest $\mathcal{O}(10^{1-5})$ physical qubits per logical qubit [36–38]—so physical qubit requirements could easily rise to the megaqubyte scale for a 10^3 lattice.

The generically dense $\hat{U}(t)$ can be efficiently constructed only approximately. For the decomposition in noncommuting terms $\hat{H} = \sum_i \hat{H}_i$, a common approximation is *trotterization*, whereby $\hat{U}(t) \approx \mathcal{U}(t) = (\prod_i e^{-i\hat{H}_i(t/N)})^N$ [39,40]. Implementing $\mathcal{U}(t)$ for a LGT may require large number of quantum gates to achieve desirable precision. For example, in Ref. [34] a 10^3 lattice calculation of the shear viscosity η in QCD with errors of 10^{-8} from trotterization and gate synthesis was estimated to require $\mathcal{O}(10^{49})$ T gates—the most expensive gate for error-correcting quantum computers. Though these estimates could be reduced by considering only the low-lying states [41,42] or by relaxing the precision requirement to the level of uncertainties from lattice truncation, gate costs are still expected to be inaccessible in the near term.

Reducing quantum resources, either by implementing smarter quantum algorithms or performing classical processing, is thus strongly motivated. Gate reductions may be possible using other approximations of $\hat{U}(t)$ [43–48]. At the cost of classical signal-to-noise problems, stochastic state preparation yields shallower circuits [49–52]. Furthermore, performing scale setting classically can reduce quantum resources [53–55]. LGT specific error correction or mitigation could also decrease costs [56,57].

In this Letter, we present a new direction for reducing quantum resources by using Hamiltonians with smaller discretization errors from finite differences. Quantum simulations can then be done at larger a, reducing the

$\mathcal{O}[(L/a)^d]$ qubits needed. We start with illustrating how to improve the commonly used Kogut-Susskind Hamiltonian H_{KS} [58] in the Symanzik improvement program [59–61], then derive time-evolution operators for the improved terms, and construct the corresponding quantum circuits, followed by an explicit demonstration for $\mathbb{Z}_2$.

Improved Hamiltonians.—For pure gauge theories, the classical Yang-Mills Hamiltonian can be written

$$H_{\mathrm{co}} = \frac{1}{2} \int d^d x \mathrm{Tr}[\mathbf{E}^2(\mathbf{x}) + \mathbf{B}^2(\mathbf{x})], \qquad (1)$$

where $\mathbf{E}(\mathbf{x})$ and $\mathbf{B}(\mathbf{x})$ are the electric and magnetic field strengths with spatial components $E_i(\mathbf{x})$ and $B_i(\mathbf{x})$, respectively. Alternatively, the magnetic energy density can be written in terms of $F_{ij}(\mathbf{x})$, the spatial-spatial field strength tensor, as $\frac{1}{2}\mathbf{B}^2(\mathbf{x}) = \frac{1}{2}\sum_{i<j} F_{ij}^2(\mathbf{x})$ with Latin indices indicating spatial directions as shown in Fig. 1. In terms of color components, $E_i(\mathbf{x}) = E_i^b(\mathbf{x})\lambda_b$ and $B_i(\mathbf{x}) = B_i^b(\mathbf{x})\lambda_b$, with λ_b being generators of the gauge group. To ensure gauge invariance, lattice Hamiltonians are built from gauge links $U_i(\mathbf{x}) = e^{igaA_i(\mathbf{x})}$ connecting lattice site $\mathbf{x}$ to its neighbor in the i spatial direction, with g being the gauge coupling and $A_i(\mathbf{x})$ the lattice gauge field [62]. By replacing the magnetic field $B_i(\mathbf{x})$ term with the plaquettes $P_{ij}(\mathbf{x})$ (see Fig. 1 for $i = x$ and $j = y$) built from $U_i(\mathbf{x})$ and the electric field $E_i(\mathbf{x})$ with the lattice electric field $L_i(\mathbf{x})$, one arrives at H_{KS} [58]:

$$H_{\mathrm{KS}} = K_{\mathrm{KS}} + V_{\mathrm{KS}},$$

$$K_{\mathrm{KS}} = \sum_{\mathbf{x},i} \frac{g_t^2}{a} \mathrm{Tr} L_i^2(\mathbf{x}), \quad V_{\mathrm{KS}} = -\sum_{\mathbf{x},i<j} \frac{2}{g_s^2 a} \mathrm{Re} \mathrm{Tr} P_{ij}(\mathbf{x}). \quad (2)$$

As temporal and spatial directions are treated differently, couplings g_t and g_s are introduced for the kinetic term K_{KS} and potential term V_{KS}, respectively. The discrepancy
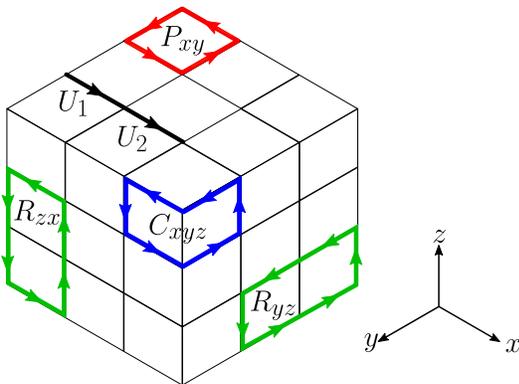
FIG. 1. 3D lattice with example contributions to H_I—the plaquette P_{xy}, rectangles R_{yz} and R_{zx}, and the bent loop C_{xyz}—and the two links U_1 and U_2 used for K_{2L}.

between H_{KS} and H_{co} is of $\mathcal{O}(a^2)$, as seen by series-expanding P_{ij} with D_i denoting the covariant derivative:

$$P_{ij} = \mathbb{1} - \frac{g_s^2 a^4}{2}\left[F_{ij}^2 + \frac{a^2}{12} F_{ij}(D_i^2 + D_j^2)F_{ij} + \mathcal{O}(a^4) \right]. \quad (3)$$

For Symanzik improvement, one adds terms to H_{KS} and adjusts couplings to cancel the discretization errors [63,64]. The above classical $\mathcal{O}(a^2)$ error from $F_{ij}(D_i^2 + D_j^2)F_{ij}$ can be canceled by including the rectangle term $R_{ij}(\mathbf{x})$ (Fig. 1), as detailed in Supplemental Material [65]. At the quantum level, $\mathcal{O}(g_s^2 a^2)$ errors arise, requiring more terms, say, the six-link bent loop terms $C_{ijk}(\mathbf{x})$ (Fig. 1).

The improved Hamiltonian can be written as $H_I = K_I + V_I$ with the improved potential term $V_I = \beta_{V0}V_{\mathrm{KS}} + \beta_{V1}V_{\mathrm{rect}} + \beta_{V2}V_{\mathrm{bent}}$ and the improved kinetic term $K_I = \beta_{K0}K_{\mathrm{KS}} + \beta_{K1}K_{2L}$ [64]. V_{rect} is defined as

$$V_{\mathrm{rect}} = \frac{2}{ag_s^2} \sum_{\mathbf{x},i<j} \mathrm{Re} \mathrm{Tr}[R_{ij}(\mathbf{x}) + R_{ji}(\mathbf{x})], \qquad (4)$$

and V_{bent} has analogous expressions to V_{rect}. To cancel the $\mathcal{O}(a^2)$ errors in K_{KS}, one adds the two-link term K_{2L}:

$$K_{2L} = \frac{g_t^2}{a} \sum_{\mathbf{x},i} \mathrm{Tr}[L_i(\mathbf{x})U_i(\mathbf{x})L_i(\mathbf{x} + a\mathbf{i})U_i^\dagger(\mathbf{x})]. \quad (5)$$

For classical improvement, the couplings should be [63,64] $\beta_{V0} = \frac{5}{3}$, $\beta_{V1} = -\frac{1}{12}$, $\beta_{V2} = 0$, $\beta_{K0} = \frac{5}{6}$, and $\beta_{K1} = \frac{1}{6}$. Perturbative improvements at the quantum level generate corrections of $\mathcal{O}(g^2 a^2)$ [61,67]. One can further nonperturbatively tune these couplings numerically. For quantum
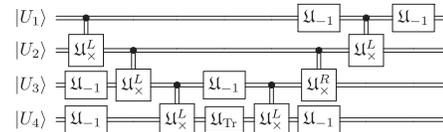
(a) $\mathcal{U}_{V_{\mathrm{KS}}}$ assuming linear register connectivity.
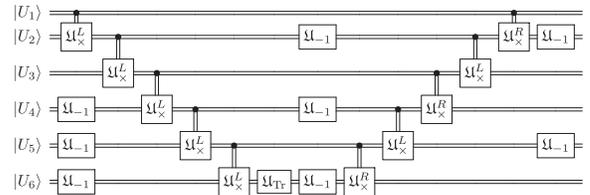
(b) $\mathcal{U}_{V_{\mathrm{rect}}}$ assuming linear register connectivity.
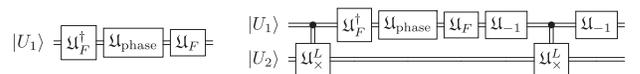
(c) $\mathcal{U}_{K_{\mathrm{KS}}}$.   (d) $\mathcal{U}_{K_{2L}}$.

FIG. 2. Quantum circuits for the time evolution of $\hat{H}_I$.

TABLE I. Number of primitive gates per link register per Trotter step neglecting boundary effects (columns 2 and 3) and implementation for $\mathbb{Z}_2$ (last column).

Gate	$N[\hat{K}_{KS} + \hat{V}_{KS}]$	$N[\hat{K}_{2L} + \hat{V}_{rect}]$	$\mathbb{Z}_2$ impl.
$\mathcal{U}_F$	2	2	H
$\mathcal{U}_{phase}$	1	1	$R_z(\theta)$
$\mathcal{U}_{Tr}$	$(d-1)/2$	$d-1$	$R_z(\theta)$
$\mathcal{U}_{-1}$	$3(d-1)$	$2 + 8(d-1)$	1
$\mathcal{U}_\times$	$6(d-1)$	$4 + 20(d-1)$	CNOT

simulations, these couplings could be extracted via analytic continuation of Euclidean calculations [55]. The resulting H_I then has leading errors of $\mathcal{O}(a^4)$ to H_{co}.

Both H_{KS} and H_I can be derived from Euclidean actions via the transfer matrix in the continuous-time limit. The Lüscher-Weisz action [60] was used to derive H_I [63,64] and has improved errors of $\mathcal{O}(a^4)$ compared to the $\mathcal{O}(a^2)$ Wilson action used to derive H_{KS} [68]. For the Lüscher-Weisz action, $a = 0.4$ fm lattices were found to have similar discretization errors to $a = 0.17$ fm lattices with the Wilson action [69]. Similar scaling is suggested by the limited direct studies of H_I and H_{KS} [70]. As the number of qubits required is $\mathcal{O}[(L/a)^d]$, using H_I may require $\gtrsim 2^d$ fewer qubits in realistic quantum simulations for a fixed discretization error compared to H_{KS}. While we occupy ourselves with pure gauge theory, future effort should consider the $\mathcal{O}(a)$ fermion Hamiltonians [71]—particularly for chiral fermions.

Circuit design.—For quantum field theory calculations, H_I is quantized by promoting the fields to operators: $U_i \to \hat{U}_i, L_i \to \hat{L}_i$. The magnetic field basis is the eigenbasis of the link operator $\hat{U}$, while its Fourier transformation gives the electric field basis $|L_i\rangle$ diagonalizing $\hat{L}_i^2$. The quantum state of a link $|U_i\rangle$ is stored in a set of qubits—a link register. Any gauge circuit can be built from a set of primitive gates [72] acting on link registers: (i) inverse gate $\mathcal{U}_{-1}|U_i\rangle = |U_i^{-1}\rangle$, (ii) left and right multiplication gates: $\mathcal{U}_\times^L|U_i\rangle|U_j\rangle = |U_i\rangle|U_iU_j\rangle$ and $\mathcal{U}_\times^R|U_i\rangle|U_j\rangle = |U_i\rangle|U_jU_i\rangle$, respectively, (iii) trace gate $\mathcal{U}_{Tr}(\theta)|U_i\rangle = e^{i\theta \mathrm{ReTr}U_i}|U_i\rangle$, (iv) Fourier gate $\mathcal{U}_F \sum_{U_i} f(U_i)|U_i\rangle = \sum_{L_i} \hat{f}(L_i)|L_i\rangle$, with

$\hat{f}$ denoting the Fourier transform of f, (v) L-phase gate $\mathcal{U}_{phase}(\theta)$ is a gauge group specific phase rotation, implemented by a diagonal matrix.

We implement the quantum circuits for $\hat{H}_I$ term by term. Optimal quantum circuits depend on the underlying architecture—in particular, connectivity. We assume register connectivity between a pair of links sharing a common site (linear register connectivity).

$\hat{V}_I$ includes $\hat{P}_{ij}(\mathbf{x})$ for every individual plaquette and the rectangles $\hat{R}_{ij}(\mathbf{x})$ for every neighboring two plaquettes. We denote the circuits for $\hat{V}_{KS}$ as $\mathcal{U}_{V_{KS}} = e^{i\theta \mathrm{ReTr}\hat{P}_{ij}(\mathbf{x})}$ [Fig. 2(a)] and for the rectangles $\mathcal{U}_{V_{rect}} = e^{i\theta \mathrm{ReTr}\hat{R}_{ij}(\mathbf{x})}$ [Fig. 2(b)], with the coupling and Trotter step encoded in θ. The circuit in Fig. 2(b) with registers appropriately changed implements $\mathcal{U}_{V_{bent}}$.

The circuits $\mathcal{U}_{K_{KS}} = e^{i\theta \mathrm{Tr}\hat{L}_i^2}$ for $\hat{K}_{KS}$ can be implemented by the L-phase gate $\mathcal{U}_{phase}$ in the electric field basis [72], as shown in Fig. 2(c). To avoid dealing with $\hat{L}$ and $\hat{U}$ operators simultaneously, we rewrite $\hat{K}_{2L}$ as

$$\hat{K}_{2L} = \frac{g_t^2}{a} \sum_{x,i} \mathrm{Tr}[\hat{R}_i(\mathbf{x})\hat{L}_i(\mathbf{x} + a\mathbf{i})], \qquad (6)$$

using the right electric field operator [19]:

$$\hat{R}_i(\mathbf{x}) \equiv \hat{U}_i^\dagger(\mathbf{x})\hat{L}_i(\mathbf{x})\hat{U}_i(\mathbf{x}) = \hat{R}_i^b(\mathbf{x})\lambda_b. \qquad (7)$$

For simplicity, we denote the two succeeding links in one direction as U_1 and U_2 following Fig. 1, and thus $\mathrm{Tr}[\hat{R}_i(\mathbf{x})\hat{L}_i(\mathbf{x} + a\mathbf{i})]$ becomes $\mathrm{Tr}[\hat{R}_1\hat{L}_2]$. For non-Abelian gauge theories, this sum of noncommuting terms ($\hat{R}_1^b\hat{L}_2^b$ with color index b) is difficult to implement. We bypass this obstacle by decomposing $\hat{R}_1\hat{L}_2$ as

$$\mathrm{Tr}(\hat{R}_1\hat{L}_2) = \mathrm{Tr}[\hat{L}_2^2 + \hat{R}_1^2 - (\hat{L}_2 - \hat{R}_1)^2]/2. \qquad (8)$$

With $\hat{R}^2 = \hat{L}^2$, the first two terms can be absorbed into $\hat{K}_{KS}$. Thus, for $\hat{K}_I$ the only new term is $\mathrm{Tr}[(\hat{L}_2 - \hat{R}_1)^2]$. Defining the evolution operator $\mathcal{U}_{K_{2L}} \equiv e^{i\theta \mathrm{Tr}(\hat{L}_2 - \hat{R}_1)^2}$ and
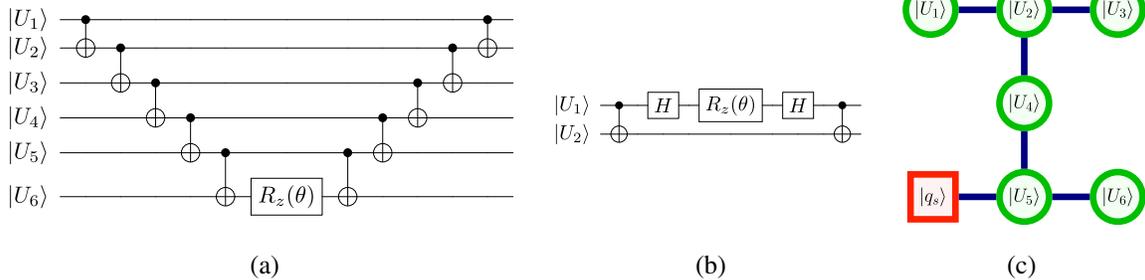
FIG. 3. $\mathcal{U}_{V_{rect}}$ (a) and $\mathcal{U}_{K_{2L}}$ (b) for $\mathbb{Z}_2$ gauge theory. (c) Link-to-qubit map on ibm_perth.
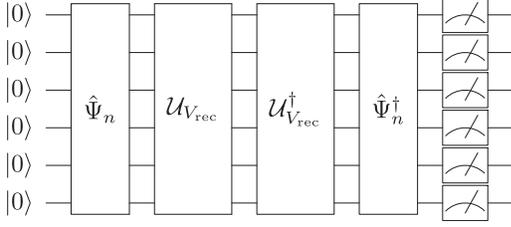
FIG. 4. $\mathcal{U}_{\rm circ}^{|n\rangle}$ for studying the errors of $\mathcal{U}_{V_{\rm rect}}$.

FIG. 5. Probability of measuring Hamming weights for selected $|\Psi_n\rangle$ compared to the noise-dominated results. In the noiseless limit, $P(w_H) = \delta_{w_H,0}$ for all $|\Psi_n\rangle$.

using $[\mathcal{U}_{K_{2L}}, \hat{U}_1 \hat{U}_2] = 0$, the matrix elements of $\mathcal{U}_{K_{2L}}$ are found to be (see Supplemental Material [65])

$$\langle U_1', U_2' | \mathcal{U}_{K_{2L}} | U_1, U_2 \rangle = \delta_{U_1'U_2',U_1U_2} \langle U_1' | e^{i\theta {\rm Tr} \hat{L}_1^2} | U_1 \rangle. \quad (9)$$

The circuit in Fig. 2(d) implements Eq. (9) by first storing the conserved quantity $U_1 U_2$ in the second register $|U_2\rangle$ via $\mathcal{U}_\times^L$ and then performing $e^{i\theta {\rm Tr} \hat{L}_1^2}$ on $|U_1\rangle$ with the sequence $\mathcal{U}_F^\dagger \mathcal{U}_{\rm phase} \mathcal{U}_F$. Finally, we ensure the conserved product of $U_1 U_2$ imposed by $\delta(U_1' U_2' - U_1 U_2)$ using the information stored in the second register via $\mathcal{U}_{-1} \mathcal{U}_\times \mathcal{U}_{-1}$.

While using $\hat{H}_I$ should require $\gtrsim 2^d$ times fewer qubits, it requires additional gates to implement evolutions with the improved terms. Since the dominant quantum errors today are from decoherence and entangling gates with error rates of $\mathcal{O}(10^{-2})$ [73–75], this increased cost may diminish the gain from using $\hat{H}_I$. We list the gate costs in terms of primitive gates in Table I for one Trotter step using either $\hat{H}_{\rm KS}$ or $\hat{H}_I$. Depending on which primitive gates dominate the circuits, the gate cost for $\hat{H}_I$ is 2–4 times that of $\hat{H}_{\rm KS}$ per link register. For the group $\mathbb{Z}_N$ and D_N [76], different primitive gates take approximately the same order of entangling native gates. Since $\hat{H}_I$ should require $\gtrsim 2^d$ fewer link registers, for the cases of $d = 2, 3$ we anticipate the same or fewer total primitive gate cost.

Demonstration.—For $\mathbb{Z}_2$ gauge theory, $\hat{H}_I$ can be mapped to Pauli matrices. Choosing the magnetic field basis, the qubit state $|0\rangle$ ($|1\rangle$) represents the element 1 (-1) of $\mathbb{Z}_2$. Implementations of the primitive gates are listed in the last column in Table I. We consider the most expensive $\mathbb{Z}_2$ gate $\mathcal{U}_{V_{\rm rect}}$ on the seven-qubit ibm_perth device [Fig. 3(c)]. The connectivity of ibm_perth prevents implementing $\mathcal{U}_{V_{\rm rect}}$ as shown in Fig. 3(a). With the mapping from links to qubits shown in Fig. 3(c), a transpiled version of the circuit with 12 CNOTs and 20 additional one-qubit gates are used. We use the benchmark value $\theta = \delta t/(g_s g_t) = 0.811411$, precluding circuit optimization when using θ values such as $\pi/2$.

To quantify quantum errors, we evolve states with $\mathcal{U}_{V_{\rm rect}}$ and its inverse, and compare the measurement with noiseless expectations, implemented as the circuit $\mathcal{U}_{\rm circ}^{|n\rangle}$ in Fig. 4. Without noise, the state preparation $\hat{\Psi}_n$ and $\mathcal{U}_{V_{\rm rect}}$ are exactly canceled by their complex conjugations; thus,
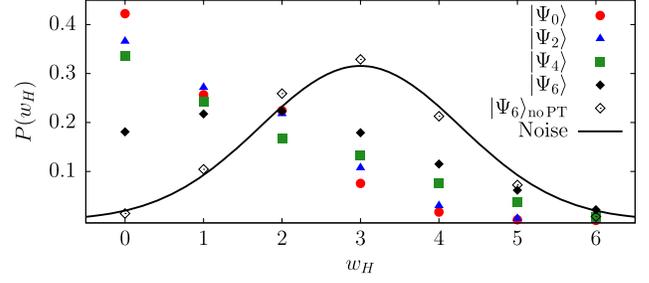
all measurements return $|0\rangle^{\otimes 6}$, and the distribution $P(w_H)$ of the Hamming weight w_H—the number of qubits measured in the $|1\rangle$ state—returns $P(w_H) = \delta_{w_H,0}$. In the noise-dominated limit where all states are equally populated, $P(w_H)$ follows the binomial distribution with six trials. We take $\mathcal{F}_{\rm rect}^{|n\rangle} \equiv \sqrt{P(w_H = 0)}$ as a definition of the quantum fidelity of $\mathcal{U}_{V_{\rm rect}}$ for the state $|\Psi_n\rangle = \hat{\Psi}_n |0\rangle^{\otimes 6}$. Determining the fidelity requires testing all the possible states $|\Psi_n\rangle$, a prohibitively expensive task [77]. Therefore, we consider a restricted set consisting of $\hat{\Psi}_n = \prod_{m \le n} H_m^\otimes$ for $n \in [0, 6]$ with m indicating the qubit to which H is applied.

To mitigate the coherent noise dominating the CNOT errors, we implement Pauli twirling [78–82], which converts coherent errors into random errors in Pauli channels and has found success in low-dimensional lattice field theories [83]. The circuits are modified by wrapping each CNOT with a set of Pauli gates $\{\mathbb{1}, X, Y, Z\}$ randomly sampled from sets satisfying

$$\left[\prod_i (\sigma_i^{b_i})^\otimes\right] {\rm CNOT} \otimes \mathbb{1}_4 \left[\prod_i (\sigma_i^{a_i})^\otimes\right] = {\rm CNOT} \otimes \mathbb{1}_4, \quad (10)$$

where the ith qubit (including spectators) was rotated by $\sigma_i^{a_i}$ before the CNOT and by $\sigma_i^{b_i}$ after. Despite the enormous number of possible circuits, prior work has found $\mathcal{O}(10)$ circuits to be sufficient for error mitigation [78]. Therefore, we implement 15 unique circuits and run each circuit 2^{13} times. We also compute $\mathcal{F}_{\rm rect}^{|6\rangle}$ without Pauli twirling to gauge its effect.

With the above setup, we obtain the distribution $P(w_H)$ in Fig. 5 for selected $|\Psi_n\rangle$ and the state-dependent fidelities $\mathcal{F}_{\rm rect}^{|n\rangle}$ (Table II), yielding an average $\mathcal{F}_{\rm rect} = 0.550$. Without Pauli twirling for $n = 6$, $P(w_H)$ is indistinguishable from

TABLE II. Measured state-dependent quantum fidelities with Pauli twirling and without it for $|\Psi_6\rangle_{\rm no\,PT}$.

$|\Psi_n\rangle$	$|\Psi_0\rangle$	$|\Psi_1\rangle$	$|\Psi_2\rangle$	$|\Psi_3\rangle$	$|\Psi_4\rangle$	$|\Psi_5\rangle$	$|\Psi_6\rangle$	$|\Psi_6\rangle_{\rm no\,PT}$
$\mathcal{F}_{\rm rect}^{|n\rangle}$	0.650	0.575	0.605	0.599	0.579	0.442	0.425	0.1194

the noise-dominated limit, while all the Pauli-twirled results are skewed toward the noiseless result, with states of lower n (and consequently less average entanglement) being closer to the desired value. Comparing the results for $|\Psi_6\rangle$ with and without Pauli twirling, we observe a fourfold improvement in fidelity—clearly demonstrating the advantage from this error mitigation.

For one Trotter step, the time evolution of $\hat{H}_I$ for a two-plaquette lattice with open boundary conditions requires at least 28 CNOTs (40 one-qubit gates): 12 CNOTs (20 one-qubit gates) for $\mathcal{U}_{V_{\text{rect}}}$, at least 12 CNOTs (two one-qubit gates) for the two $\mathcal{U}_{V_{\text{KS}}}$ and four CNOTs (six one-qubit gates) for the two $\mathcal{U}_{K_{2L}}$, along with 12 one-qubit gates for $\mathcal{U}_{K_{\text{KS}}}$. Assuming that the average fidelity depends on the total number of CNOT gates, we can estimate the single-Trotter-step fidelity for $\hat{H}_I$: $\mathcal{F}_\delta \lesssim (\mathcal{F}_{\text{rect}})^{28/12} \approx 0.25$. Thus, current devices are inadequate for real-time computations. However, given the expected hardware improvements in the coming years [36–38], $\mathcal{F}_\delta$ will be improved, allowing simulations of a two-plaquette lattice for $\mathbb{Z}_2$ gauge theory and direct comparisons between Hamiltonians. Alternatively, classical simulators could explore lattices up to 7^2 [84] to test improved Hamiltonians.

In this Letter, we designed quantum circuits for simulating the improved Hamiltonian $\hat{H}_I$. Comparing to the commonly used $\hat{H}_{\text{KS}}$, $\hat{H}_I$ should allow quantum simulations with $\gtrsim 2^d$ fewer qubits. With this reduction, we expect the gate count to be comparable to or less than that of $\hat{H}_{\text{KS}}$ for theories with $d \geq 2$ despite increases of gate costs per link. For near-term numerical demonstrations, we constructed the circuits for $\hat{H}_I$ of the $\mathbb{Z}_2$ gauge theory and found that for ibm_perth the fidelity of the 12 CNOT improved potential term is $\lesssim 0.550$. Our results suggest that, alongside hardware developments, improved Hamiltonians can accelerate quantum simulations by years by reducing the number of qubits required, with optimistic prospects for $2 + 1d$ $\mathbb{Z}_2$ simulations in the near future.

[*] carena@fnal.gov

[†] hlamm@fnal.gov

[‡] Corresponding author.
yingying@fnal.gov

[§] wanqiangl@uchicago.edu

[1] A. Yamamoto, Lattice QCD in curved spacetimes, Phys. Rev. D **90**, 054510 (2014).

[2] H. Lamm, S. Lawrence, and Y. Yamauchi (NuQS Collaboration), Parton physics on a quantum computer, Phys. Rev. Research **2**, 013272 (2020).

[3] M. Kreshchuk, W. M. Kirby, G. Goldstein, H. Beauchemin, and P. J. Love, Quantum simulation of quantum field theory in the light-front formulation, Phys. Rev. A **105**, 032418 (2022).

[4] M. Echevarria, I. Egusquiza, E. Rico, and G. Schnell, Quantum simulation of light-front parton correlators, Phys. Rev. D **104**, 014512 (2021).

[5] T. D. Cohen, H. Lamm, S. Lawrence, and Y. Yamauchi (NuQS Collaboration), Quantum algorithms for transport coefficients in gauge theories, Phys. Rev. D **104**, 094514 (2021).

[6] R. P. Feynman, Simulating physics with computers, Int. J. Theor. Phys. **21**, 467 (1982).

[7] S. P. Jordan, H. Krovi, K. S. Lee, and J. Preskill, BQP-completeness of scattering in scalar quantum field theory, Quantum **2**, 44 (2018).

[8] M. C. Bañuls et al., Simulating lattice gauge theories within quantum technologies, Eur. Phys. J. D **74**, 165 (2020).

[9] E. Gustafson, H. Kawai, H. Lamm, I. Raychowdhury, H. Singh, J. Stryker, and J. Unmuth-Yockey, Exploring digitizations of quantum fields for quantum devices, Snowmass 2021 LOI TF10-97(2020), https://www.snowmass21.org/docs/files/summaries/TF/SNOWMASS21-TF10_TF0-CompF6_CompF0_Hank_Lamm-079.pdf.

[10] D. C. Hackett, K. Howe, C. Hughes, W. Jay, E. T. Neil, and J. N. Simone, Digitizing gauge fields: Lattice Monte Carlo results for future quantum computers, Phys. Rev. A **99**, 062341 (2019).

[11] A. Alexandru, P. F. Bedaque, S. Harmalkar, H. Lamm, S. Lawrence, and N. C. Warrington (NuQS Collaboration), Gluon field digitization for quantum computers, Phys. Rev. D **100**, 114501 (2019).

[12] A. Yamamoto, Real-time simulation of $(2 + 1)$-dimensional lattice gauge theory on qubits, Prog. Theor. Exp. Phys. **2021**, 013B06 (2021).

[13] Y. Ji, H. Lamm, and S. Zhu (NuQS Collaboration), Gluon field digitization via group space decimation for quantum computers, Phys. Rev. D **102**, 114513 (2020).

[14] J. F. Haase, L. Dellantonio, A. Celi, D. Paulson, A. Kan, K. Jansen, and C. A. Muschik, A resource efficient approach for quantum and classical simulations of gauge theories in particle physics, Quantum **5**, 393 (2021).

[15] E. Zohar, J. I. Cirac, and B. Reznik, Simulating Compact Quantum Electrodynamics with Ultracold Atoms: Probing Confinement and Nonperturbative Effects, Phys. Rev. Lett. **109**, 125302 (2012).

[16] E. Zohar, J. I. Cirac, and B. Reznik, Cold-Atom Quantum Simulator for SU(2) Yang-Mills Lattice Gauge Theory, Phys. Rev. Lett. **110**, 125304 (2013).

[17] E. Zohar, J. I. Cirac, and B. Reznik, Quantum simulations of gauge theories with ultracold atoms: Local gauge invariance from angular momentum conservation, Phys. Rev. A **88**, 023617 (2013).

[18] E. Zohar and M. Burrello, Formulation of lattice gauge theories for quantum simulations, Phys. Rev. D **91**, 054506 (2015).

[19] E. Zohar, J. I. Cirac, and B. Reznik, Quantum simulations of lattice gauge theories using ultracold atoms in optical lattices, Rep. Prog. Phys. **79**, 014401 (2016).

[20] E. Zohar, A. Farace, B. Reznik, and J. I. Cirac, Digital lattice gauge theories, Phys. Rev. A **95**, 023604 (2017).

[21] N. Klco, M. J. Savage, and J. R. Stryker, SU(2) non-Abelian gauge field theory in one dimension on digital quantum computers, Phys. Rev. D **101**, 074512 (2020).

[22] A. Ciavarella, N. Klco, and M. J. Savage, A trailhead for quantum simulation of SU(3) Yang-Mills lattice gauge theory in the local multiplet basis, Phys. Rev. D **103**, 094501 (2021).

[23] J. Bender, E. Zohar, A. Farace, and J. I. Cirac, Digital quantum simulation of lattice gauge theories in three spatial dimensions, New J. Phys. **20**, 093001 (2018).

[24] U.-J. Wiese, Towards quantum simulating QCD, Nucl. Phys. **A931**, 246 (2014).

[25] D. Luo, J. Shen, M. Highman, B. K. Clark, B. DeMarco, A. X. El-Khadra, and B. Gadway, A framework for simulating gauge theories with dipolar spin systems, Phys. Rev. A **102**, 032617 (2020).

[26] R. C. Brower, D. Berenstein, and H. Kawai, Lattice gauge theory for a quantum computer, Proc. Sci., LATTICE2019 (**2019**) 112.

[27] S. V. Mathis, G. Mazzola, and I. Tavernelli, Toward scalable simulations of lattice gauge theories on quantum computers, Phys. Rev. D **102**, 094501 (2020).

[28] H. Singh, Qubit $O(N)$ nonlinear sigma models, Phys. Rev. D **105**, 114509 (2022).

[29] H. Singh and S. Chandrasekharan, Qubit regularization of the $O(3)$ sigma model, Phys. Rev. D **100**, 054505 (2019).

[30] A. J. Buser, T. Bhattacharya, L. Cincio, and R. Gupta, State preparation and measurement in a quantum simulation of the O(3) sigma model, Phys. Rev. D **102**, 114514 (2020).

[31] I. Raychowdhury and J. R. Stryker, Solving Gauss's law on digital quantum computers with loop-string-hadron digitization, Phys. Rev. Research **2**, 033039 (2020).

[32] I. Raychowdhury and J. R. Stryker, Loop, string, and hadron dynamics in SU(2) Hamiltonian lattice gauge theories, Phys. Rev. D **101**, 114502 (2020).

[33] Z. Davoudi, I. Raychowdhury, and A. Shaw, Search for efficient formulations for Hamiltonian simulation of non-abelian lattice gauge theories, Phys. Rev. D **104**, 074505 (2021).

[34] A. Kan and Y. Nam, Lattice quantum chromodynamics and electrodynamics on a universal quantum computer, arXiv:2107.12769.

[35] A. Alexandru, P. F. Bedaque, R. Brett, and H. Lamm, The spectrum of qubitized QCD: Glueballs in a $S(1080)$ gauge theory, Phys. Rev. D **105**, 114508 (2022).

[36] Scaling IonQ's quantum computers: The roadmap (2020).

[37] IBM's roadmap for building an open quantum software ecosystem (2021).

[38] H. Neven, Day 1 opening keynote by Hartmut Neven (quantum summer symposium 2020) (2020).

[39] H. F. Trotter, On the product of semi-groups of operators, Proc. Am. Math. Soc. **10**, 545 (1959).

[40] M. Suzuki, Decomposition formulas of exponential operators and lie exponentials with some applications to quantum mechanics and statistical physics, J. Math. Phys. (N.Y.) **26**, 601 (1985).

[41] B. Şahinoğlu and R. D. Somma, Hamiltonian simulation in the low energy subspace, arXiv:2006.02660.

[42] T. Hatomura, State-dependent error bound for digital quantum simulation of driven systems, Phys. Rev. A **105**, L050601 (2022).

[43] E. Campbell, Random Compiler for Fast Hamiltonian Simulation, Phys. Rev. Lett. **123**, 070503 (2019).

[44] C. Cirstoiu, Z. Holmes, J. Iosue, L. Cincio, P. J. Coles, and A. Sornborger, Variational fast forwarding for quantum simulation beyond the coherence time, npj Quantum Inf. **6**, 82 (2020).

[45] J. Gibbs, K. Gili, Z. Holmes, B. Commeau, A. Arrasmith, L. Cincio, P. J. Coles, and A. Sornborger, Long-time simulations with high fidelity on quantum hardware, arXiv:2102.04313.

[46] Y.-X. Yao, N. Gomes, F. Zhang, T. Iadecola, C.-Z. Wang, K.-M. Ho, and P. P. Orth, Adaptive variational quantum dynamics simulations, PRX Quantum **2**, 030307 (2021).

[47] D. W. Berry, A. M. Childs, R. Cleve, R. Kothari, and R. D. Somma, Simulating Hamiltonian Dynamics with a Truncated Taylor Series, Phys. Rev. Lett. **114**, 090502 (2015).

[48] G. H. Low and I. L. Chuang, Hamiltonian simulation by qubitization, Quantum **3**, 163 (2019).

[49] H. Lamm and S. Lawrence, Simulation of Nonequilibrium Dynamics on a Quantum Computer, Phys. Rev. Lett. **121**, 170501 (2018).

[50] S. Harmalkar, H. Lamm, and S. Lawrence (NuQS Collaboration), Quantum simulation of field theories without state preparation, arXiv:2001.11490.

[51] E. J. Gustafson and H. Lamm, Toward quantum simulations of $\mathbb{Z}_2$ gauge theory without state preparation, Phys. Rev. D **103**, 054507 (2021).

[52] Y. Yang, B.-N. Lu, and Y. Li, Accelerated quantum Monte Carlo with mitigated error on noisy quantum computer, PRX Quantum **2**, 040361 (2021).

[53] K. Osterwalder and R. Schrader, Axioms for euclidean Green's functions, Commun. Math. Phys. **31**, 83 (1973).

[54] K. Osterwalder and R. Schrader, Axioms for euclidean Green's functions. 2., Commun. Math. Phys. **42**, 281 (1975).

[55] M. Carena, H. Lamm, Y.-Y. Li, and W. Liu, Lattice renormalization of quantum simulations, Phys. Rev. D **104**, 094519 (2021).

[56] A. Rajput, A. Roggero, and N. Wiebe, Quantum error correction with gauge symmetries, arXiv:2112.05186.

[57] N. Klco and M. J. Savage, Hierarchical qubit maps and hierarchically implemented quantum error correction, Phys. Rev. A **104**, 062425 (2021).

[58] J. Kogut and L. Susskind, Hamiltonian formulation of Wilson's lattice gauge theories, Phys. Rev. D **11**, 395 (1975).

[59] K. Symanzik, Continuum limit and improved action in lattice theories. 1. Principles and φ^4 Theory, Nucl. Phys. **B226**, 187 (1983).

[60] M. Luscher and P. Weisz, On-shell improved lattice gauge theories, Commun. Math. Phys. **97**, 59 (1985); **98**, 433(E) (1985).

[61] M. Luscher and P. Weisz, Computation of the action for on-shell improved lattice gauge theories at weak coupling, Phys. Lett. **158B**, 250 (1985).

[62] K. G. Wilson, Confinement of quarks, Phys. Rev. D **10**, 2445 (1974).

[63] X.-Q. Luo, S.-H. Guo, H. Kroger, and D. Schutte, Improved lattice gauge field Hamiltonian, Phys. Rev. D **59**, 034503 (1999).

[64] J. Carlsson and B. H. J. McKellar, Direct improvement of Hamiltonian lattice gauge theory, Phys. Rev. D **64**, 094503 (2001).

[65] See Supplemental Material at http://link.aps.org/supplemental/10.1103/PhysRevLett.129.051601 for brief reviews of derivations for the improved terms and left/right operators of the group, and for our derivations of the kinetic term circuit, which includes Refs. [18,19,66].

[66] A. F. Izmaylov, On construction of projection operators, J. Phys. Chem. A **123**, 3429 (2019).

[67] G. P. Lepage, Redesigning lattice QCD, in *Perturbative and Nonperturbative Aspects of Quantum Field Theory*, Lecture Notes in Physics Vol. 479 (Springer, Berlin, Heidelberg, 1977), pp. 1–48, 10.1007/bfb0104288.

[68] M. Creutz, Gauge fixing, the transfer matrix, and confinement on a lattice, Phys. Rev. D **15**, 1128 (1977).

[69] M. G. Alford, W. Dimm, G. P. Lepage, G. Hockney, and P. B. Mackenzie, Lattice QCD on small computers, Phys. Lett. B **361**, 87 (1995).

[70] J. Carlsson, Improvement and analytic techniques in Hamiltonian lattice gauge theory, Other thesis, School of Physics, The University of Melbourne, 2003, arXiv:hep-lat/0309138.

[71] D. Spitz and J. Berges, Schwinger pair production and string breaking in non-Abelian gauge theory from real-time lattice improved Hamiltonians, Phys. Rev. D **99**, 036020 (2019).

[72] H. Lamm, S. Lawrence, and Y. Yamauchi (NuQS Collaboration), General methods for digital quantum simulation of gauge theories, Phys. Rev. D **100**, 034518 (2019).

[73] K. Wei, E. Magesan, I. Lauer, S. Srinivasan, D. Bogorin, S. Carnevale, G. Keefe, Y. Kim, D. Klaus, W. Landers *et al.*, Quantum crosstalk cancellation for fast entangling gates and improved multi-qubit performance, arXiv:2106.00675.

[74] L. Lao, A. Korotkov, Z. Jiang, W. Mruczkiewicz, T. E. O'Brien, and D. E. Browne, Software mitigation of coherent two-qubit gate errors, Quantum Sci. Technol. **7**, 025021 (2022).

[75] L. Howe, M. Castellanos-Beltran, A. J. Sirois, D. Olaya, J. Biesecker, P. D. Dresselhaus, S. P. Benz, and P. F. Hopkins, Digital control of a superconducting qubit using a Josephson pulse generator at 3 K, PRX Quantum **3**, 010350 (2022).

[76] M. S. Alam, S. Hadfield, H. Lamm, and A. C. Y. Li, Quantum simulation of dihedral gauge theories, Phys. Rev. D **105**, 114501 (2022).

[77] I. L. Chuang and M. A. Nielsen, Prescription for experimental determination of the dynamics of a quantum black box, J. Mod. Opt. **44**, 2455 (1997).

[78] A. Erhard, J. J. Wallman, L. Postler, M. Meth, R. Stricker, E. A. Martinez, P. Schindler, T. Monz, J. Emerson, and R. Blatt, Characterizing large-scale quantum computers via cycle benchmarking, Nat. Commun. **10**, 5347 (2019).

[79] Y. Li and S. C. Benjamin, Efficient Variational Quantum Simulator Incorporating Active Error Minimization, Phys. Rev. X **7**, 021050 (2017).

[80] S. Endo, S. C. Benjamin, and Y. Li, Practical Quantum Error Mitigation for Near-Future Applications, Phys. Rev. X **8**, 031027 (2018).

[81] M. R. Geller and Z. Zhou, Efficient error models for fault-tolerant architectures and the pauli twirling approximation, Phys. Rev. A **88**, 012314 (2013).

[82] J. J. Wallman and J. Emerson, Noise tailoring for scalable quantum computation via randomized compiling, Phys. Rev. A **94**, 052325 (2016).

[83] K. Yeter-Aydeniz, Z. Parks, A. Nair, E. Gustafson, A. F. Kemper, R. C. Pooser, Y. Meurice, and P. Dreher, Measuring NISQ gate-based qubit stability using a $1+1$ field theory and cycle benchmarking, arXiv:2201.02899.

[84] E. Gustafson *et al.*, Large scale multi-node simulations of $\mathbb{Z}_2$ gauge theory quantum circuits using Google Cloud Platform, in *Proceedings of the IEEE/ACM Second International Workshop on Quantum Computing Software* (IEEE, 2021), arXiv:2110.07482.